The Astrophysical Journal, 906:135 (7pp), 2021 January 10 https://doi.org/10.3847/1538-4357/abc750

Chandra Detection of Three X-Ray Bright Quasars at $z > 5$

Jiang-Tao Li[1], Feige Wang[2,8], Jinyi Yang[2,9], Yuchen Zhang[1], Yuming Fu[3], Fuyan Bian[4], Joel N. Bregman[1], Xiaohui Fan[2], Qiong Li[1,5,6], Xue-Bing Wu[3,5], and Xiaodi Yu[7]
[1] Department of Astronomy, University of Michigan, 311 West Hall, 1085 S. University Avenue, Ann Arbor, MI, 48109-1107, USA; pandataotao@gmail.com
[2] Steward Observatory, University of Arizona, 933 North Cherry Avenue, Tucson, AZ 85721, USA
[3] Department of Astronomy, School of Physics, Peking University, Beijing 100871, People's Republic of China
[4] European Southern Observatory, Alonso de Córdova 3107, Casilla 19001, Vitacura, Santiago 19, Chile
[5] Kavli Institute for Astronomy and Astrophysics, Peking University, Beijing 100871, People's Republic of China
[6] Tsinghua Center of Astrophysics & Department of Astronomy, Tsinghua University, Beijing 100084, People's Republic of China
[7] Department of Astronomy and Institute of Theoretical Physics and Astrophysics, Xiamen University, Xiamen, Fujian 361005, People's Republic of China
Received 2020 September 18; revised 2020 October 20; accepted 2020 November 2; published 2021 January 18

Abstract

We report Chandra detection of three UV-bright radio-quiet quasars at $z \gtrsim 5$. We have collected a sufficient number of photons to extract an X-ray spectrum of each quasar to measure their basic X-ray properties, such as the X-ray flux, power-law photon index (Γ), and optical-to-X-ray spectral slope ($\alpha_{\rm OX}$). J074749+115352 at $z = 5.26$ is the X-ray brightest radio-quiet quasar at $z > 5$. It may have a short timescale variation (on a timescale of ~3800 s in the observer's frame, or ~600 s in the rest frame), which is, however, largely embedded in the statistical noise. We extract phase folded spectra of this quasar. There are two distinguishable states: a "high soft" state with an average X-ray flux ~2.7 times the "low hard" state, and a significantly steeper X-ray spectral slope ($\Gamma = 2.40^{+0.33}_{-0.32}$ versus $1.78^{+0.25}_{-0.24}$). We also compare the three quasars detected in this paper to other quasar samples. We find that J074749+115352, with an SMBH mass of $M_{\rm SMBH} \approx 1.8 \times 10^9\,M_\odot$ and an Eddington ratio of $\lambda_{\rm Edd} \approx 2.3$, is extraordinarily X-ray bright. It has an average $\alpha_{\rm OX} = -1.46 \pm 0.02$ and a 2–10 keV bolometric correction factor of $L_{\rm bol}/L_{\rm 2-10\ keV} = 42.4 \pm 5.8$, both significantly depart from some well defined scaling relations. We compare Γ of the three quasars to other samples at different redshifts, and do not find any significant redshift evolution based on the limited sample of $z > 5$ quasars with reliable measurements of the X-ray spectral properties.

Unified Astronomy Thesaurus concepts: X-ray quasars (1821); High-redshift galaxies (734); Early universe (435); Supermassive black holes (1663)

1. Introduction

Many supermassive black halos (SMBHs) located at the center of galaxies gained a significant fraction of their mass at high redshift. In particular, there are two quasars at $z > 7.5$ with a billion solar mass black halos (BHs) detected (Bañados et al. 2018; Yang et al. 2020). There are also some extremely massive SMBHs detected at $z > 6$ (Wu et al. 2015), with a mass comparable to the most massive ones in the local universe ($M_{\rm SMBH} \gtrsim 10^{10}{\rm M}_\odot$, e.g., McConnell et al. 2011; van den Bosch et al. 2012). The existence of such massive BHs at such a small age of the universe (<1 Gyr) is challenging to the theory of the growth of SMBHs and their coevolution with the host galaxies (e.g., Smidt et al. 2018).

X-ray observations provide important information on the inner accretion disk and hot corona close to the SMBH. There are many studies of the redshift evolution of the accretion physics of SMBHs based on X-ray measurements of some key parameters (e.g., the X-ray photon index Γ or the spectral slope between the rest frame UV and X-ray bands $\alpha_{\rm OX}$) or some well defined scaling relations (such as the relation between the rest frame UV luminosity $L_{2500\,\text{Å}}$ and $\alpha_{\rm OX}$). The major conclusion based on some very limited samples (small sample size and/or poor X-ray data) is that the accretion physics does not show significant redshift dependence up to $z \gtrsim 7$, where the most distant quasars have been detected (e.g., Nanni et al. 2017; Salvestrini et al. 2019; Vito et al. 2019; Pons et al. 2020; Wang et al. 2020b).

Quasars at $z > 5$ typically have a low X-ray flux of $< 10^{-14}\,{\rm ergs\,s^{-1}\,cm^{-2}}$. Their X-ray properties are thus often poorly constrained or estimated based on a few assumptions (e.g., $L_{\rm X}$ estimated from the broadband count rate assuming a fixed Γ; e.g., J.-T. Li et al. 2020, in preparation; Wang et al. 2020b). In particular, X-ray timing analyses of AGNs provide critical information on the geometry of the accretion disk and corona, as well as the emitting mechanisms close to the SMBH (e.g., González-Martín & Vaughan 2012; Jin et al. 2020, 2021). However, due to the poor counting statistic, X-ray timing analyses of high-z quasars are often difficult, and most of the existing timing analyses are on long timescales between different observations (e.g., Timlin et al. 2020). We therefore need higher quality X-ray data to directly measure the X-ray properties of some well defined examples.

In this paper, we present new Chandra observations of three UV-bright quasars at $z \gtrsim 5$. This redshift marks the end of the earliest fast growth stage of some of the most massive SMBHs at higher redshifts, as the average SMBH growth rate seems to slow down at lower redshifts (e.g., Willott et al. 2010; Trakhtenbrot et al. 2011). A comparison of X-ray observations of quasars at this redshift to the small number of existing high-quality X-ray observations of quasars at lower and higher redshifts will thus help us to understand how the accretion of SMBHs evolve over cosmic time.

The present paper is organized as follows. In Section 2, we present the basic reduction and spectral analysis of our Chandra

[8] NHFP Hubble Fellow.
[9] Strittmatter Fellow.

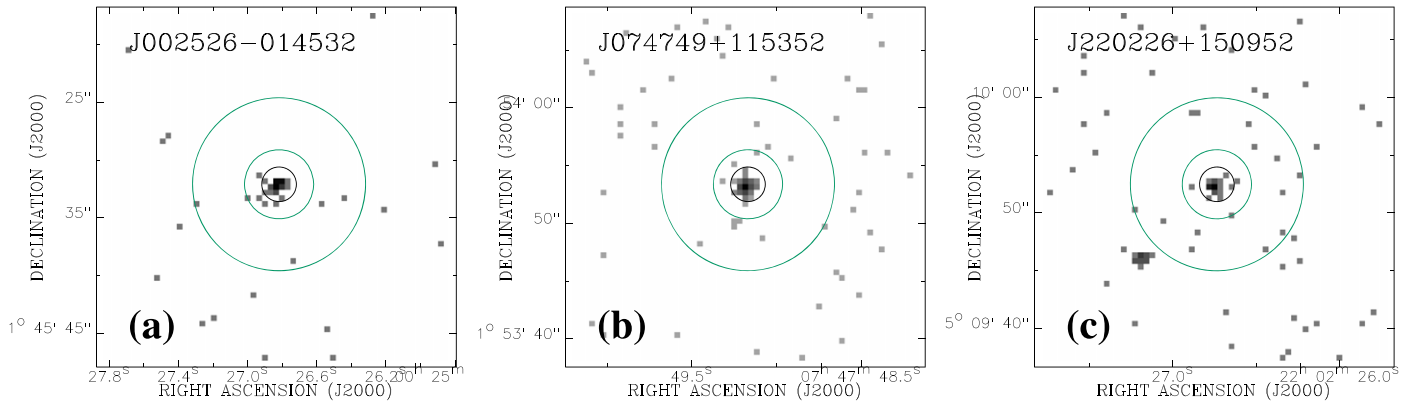

Figure 1. 0.5–7 keV Chandra count images of the three quasars studied in this paper, with their names denoted on the top left of each panel. The small circle and larger annulus in each panel are the regions used to extract the source and background spectra (Figure 2), as well as the light curve and period folded spectra of J074749+115352 (Figure 3), respectively.

Table 1
Properties of the Selected Most Luminous $z = 5$–6 Quasars and Their Chandra Observations

Name	z	M_{1450} mag	$L_{2500\ \text{Å}}$ 10^{32} erg s^{-1} Hz^{-1}	$N_{\rm H}$ 10^{20} cm^{-2}	ObsID	Obs Date	$t_{\rm exp}$ ks
J002526.84-014532.51	5.07	−28.70	1.72	2.92	22586	2019-10-30	14.58
J074749.18+115352.46	5.26	−28.04	0.94	3.83	22587	2020-01-05	29.58
J220226.77+150952.38	5.07	−28.02	0.92	5.19	22588	2019-09-19	27.90

Note. Properties of the quasars are obtained from Wang et al. (2016). The redshifts are measured with the available UV and optical emission lines from high-quality ground-based spectra. M_{1450} is the absolute magnitude at 1450 Å. $L_{2500\ \text{Å}}$ is the monochromatic luminosity at 2500 Å, and is computed from M_{1450} assuming a power-law spectral index of $\alpha = -0.5$ in UV band. $N_{\rm H}$ is the Galactic foreground absorption column density toward the quasar obtained from the HEASARC webtools using the HI4PI full-sky H I map (HI4PI Collaboration et al. 2016). The last three columns are the observational ID, start date, and effective exposure time after data calibration ($t_{\rm exp}$) of the Chandra observations.

data. For the X-ray brightest quasar in our sample, J074749 +115352, we also conduct the first timing analysis on a few kilosecond timescales (in the observer's frame) for an object at such high redshift. In Section 3, we estimate the SMBH mass of J074749+115352 based on the Mg II line in a near-IR spectrum, followed by discussions on its spectral-timing properties, as well as a comparison of the three quasars studied in this paper to other quasar samples. Our conclusions are summarized in Section 4. Throughout the paper, we adopt a flat cosmology model with $H_0 = 70\,{\rm km\,s^{-1}\,Mpc^{-1}}$, $\Omega_{\rm M} = 0.3$, $\Omega_\Lambda = 0.7$, and $q_0 = -0.55$. All the errors computed in this paper are quoted at a 1σ confidence level.

2. Observations and Data Analysis

The three quasars studied in this paper are selected from a large $z \sim 5$ UV-bright quasar sample developed in a few papers (Wang et al. 2016; Yang et al. 2016, 2017). We selected the most luminous ($M_{1450} \lesssim -28$) radio-quiet quasars for follow-up Chandra observations, which was approved in Cycle 21 (PI: Li) and taken from October 2019 to January 2020. Basic quasar properties and the corresponding Chandra observation information are summarized in Table 1.

The quasars in all of the Chandra observations (in imaging mode) are located on ACIS-S3. We reduce the data in a uniform manner with CIAO v4.11 and CALDB v4.8.5. We reprocess the evt1 file in a standard way using the CIAO tool *chandra_repro*. We then define a $r = 5''$ circular region centered at the initial optical position of the quasar, and compute the centroid position of the full band (0.5–7 keV) unbinned X-ray image. This step is conducted iteratively with smaller radius of the circular region ($r = 3''$ and $2''$), in order to accurately determine the X-ray position of the object. We then extract the source and background spectra with the CIAO tool *specextract* from a $r = 1\farcs5$ circular region and a $r = 3''$–$7\farcs5$ annulus centered at the X-ray source position computed above (Figure 1). In order to characterize the overall shape of the broadband X-ray spectra with the limited number of counts, we regroup the spectra with at least three counts in each bin (Figure 2). The spectra are analyzed with XSpec v12.9.1. We adopt the Cash statistic and assume a redshifted power-law model *zpowerlw* subjected to Galactic foreground absorption described with the model *tbabs* at a column density of $N_{\rm H}$ as listed in Table 1. At high redshifts (e.g., $z \sim 5$ for quasars studied here), the observed X-ray photons at >0.5 keV correspond to a rest frame energy of >3 keV, where the intrinsic absorption is typically negligible. We do not find any significant evidence for additional absorption, so do not include such a component in our spectral analysis. The intrinsic extinction corrected X-ray flux and the corresponding errors are calculated with the convolution model *cflux*. We list the X-ray properties of the quasars obtained from our analysis in Table 2. When computing the rest frame UV (at 2500 Å) to X-ray (at 2 keV) spectral index $\alpha_{\rm OX}$ from the absolute magnitude at 1450 Å(M_{1450}) and the measured full band X-ray luminosity, we adopt a UV spectral index of $\alpha = -0.5$ (a common assumption in similar studies, e.g., Nanni et al. 2017; Wang et al. 2020b) and the measured X-ray photon index Γ (Table 2). The measured soft X-ray flux $F_{0.5\text{–}2\ \rm keV}$ is then converted to the rest frame 2–10 keV luminosity $L_{2\text{–}10\ \rm keV}$.

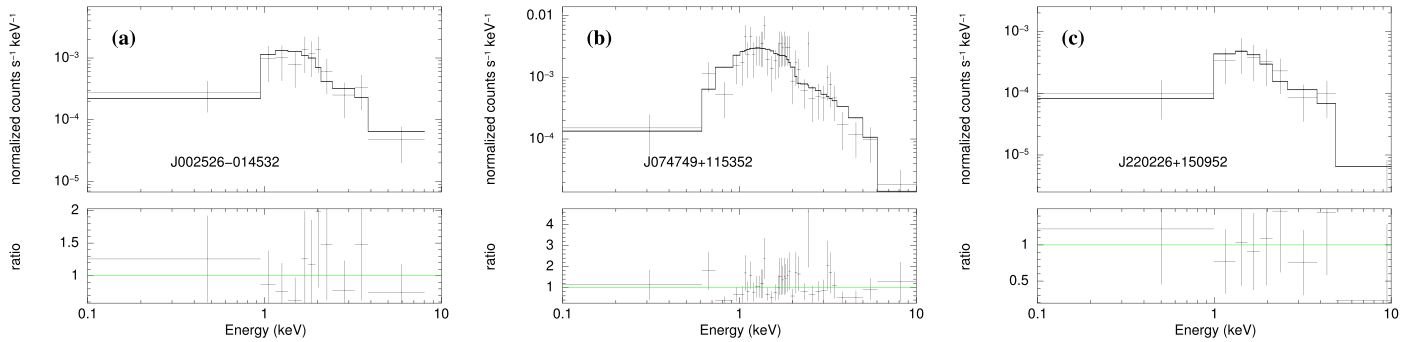

Figure 2. The Chandra spectrum of each quasar fitted with a power-law model subjected to the Milky Way foreground extinction ($N_{\rm H}$ in Table 1). The minimum count number in each bin is three.

Table 2
Measured X-Ray Properties of the Quasars

Name	$cts_{\rm S}$	$cts_{\rm H}$	$cts_{\rm F}$	$S/N_{\rm S}$	$S/N_{\rm H}$	$S/N_{\rm F}$	$F_{0.5-2\ \rm keV}$ 10^{-14}erg s^{-1} cm^{-2}	$L_{2-10\ \rm keV}$ 10^{45}erg s^{-1}	Γ	$\alpha_{\rm OX}$
J002526	19.8	13.0	32.8	4.4	3.6	5.7	$1.41^{+0.37}_{-0.38}$	$4.16^{+1.08}_{-1.13}$	$1.80^{+0.34}_{-0.33}$	$-1.70^{+0.04}_{-0.05}$
J074749	92.9	43.8	136.7	9.6	6.6	11.7	$3.49^{+0.44}_{-0.45}$	12.2 ± 1.6	2.07 ± 0.17	-1.46 ± 0.02
High	30.0	9.0	38.9	5.5	3.0	6.2	$5.86^{+1.36}_{-1.41}$	$22.9^{+5.3}_{-5.5}$	$2.40^{+0.33}_{-0.32}$	-1.42 ± 0.04
Low	37.0	22.9	59.9	6.1	4.8	7.7	$2.20^{+0.42}_{-0.43}$	$6.95^{+1.34}_{-1.38}$	$1.78^{+0.25}_{-0.24}$	-1.51 ± 0.03
J220226	12.8	10.6	23.4	3.5	3.1	4.7	$0.50^{+0.16}_{-0.17}$	$1.41^{+0.44}_{-0.47}$	$1.64^{+0.42}_{-0.41}$	$-1.75^{+0.05}_{-0.06}$

Note. "High" and "Low" indicate the X-ray properties measured in the high soft and low hard states of J074749+115352, respectively. We list them together with the X-ray properties measured from the data of J074749+115352. The subscripts "S," "H," and "F" denote soft (0.5–2 keV), hard (2–7 keV), and full (0.5–7 keV) bands, respectively, all in the observer's frame. *cts* is the net count number after subtracting the local background. S/N is the detection signal-to-noise ratio. $F_{0.5-2\ \rm keV}$ is the observed 0.5–2 keV flux. $L_{2-10\ \rm keV}$ is the rest frame 2–10 keV luminosity. Γ is the X-ray photon index obtained from spectral fitting. $\alpha_{\rm OX}$ is the optical-to-X-ray spectral slope obtained from the rest frame monochromatic UV luminosity $L_{2500\ \text{Å}}$ and the measured monochromatic X-ray luminosity at 2 keV. For the "High" and "Low" states of J074749+115352, we use the same $L_{2500\ \text{Å}}$ to compute $\alpha_{\rm OX}$, which does not account for the variation of the UV flux, thus it is just listed for comparison.

All of the three quasars have been firmly detected at a $>3\sigma$ confidence level in both the soft (0.5–2 keV) and hard (2–7 keV) X-ray bands (Table 2; Figure 1). The location of the X-ray source matches the optical counterpart well, with an offset of $\leqslant 0\farcs5$ for each quasar. This offset is smaller than the angular resolution of Chandra. It is thus unlikely to misidentify the quasar with a foreground object. We have collected >20 net counts (after subtracting the local background) from each quasar, which allows us to extract a spectrum for each of them (Figure 2). The spectra of all of the three quasars can be fitted with a power law whose photon index can be well constrained. The rest frame 2–10 keV luminosities of all of the quasars are $L_{2-10\ \rm keV} > 10^{45}$ erg s^{-1} ($>10^{46}$ erg s^{-1} for J074749.18+115352.46; hereafter J074749+115352), much higher than any stellar X-ray sources in the host galaxy. We thus confirm a robust X-ray detection of the quasars with a negligible chance of misidentification.

The observed 0.5–2 keV flux of J074749+115352 is $F_{0.5-2\ \rm keV} = 3.49^{+0.44}_{-0.45} \times 10^{-14}$ erg s^{-1} cm^{-2}. To our knowledge, this is the X-ray brightest radio-quiet quasar at $z > 5$, only after two radio-loud blazars (Q0906+6930 at $z = 5.48$, Romani 2006; SDSS J013127.34-032100.1 at $z = 5.18$, An & Romani 2020) and a radio-loud nonblazar quasar CFHQS J142952+544717 at $z = 6.18$ recently detected in X-ray by Medvedev et al. (2020) with eROSITA (the X-ray brightest quasar at $z > 5$, with an observed 0.3–2 keV flux of $8.2^{+3.7}_{-2.7} \times 10^{-14}$ erg s^{-1} cm^{-2}). Medvedev et al. (2020) have detected only nine counts (with an expected background contribution of ≈ 0.8 counts) from a $r = 30''$ circular region centered at the optical position of CFHQS J142952+544717. For comparison, we have detected 136.7 net counts from a $r = 1\farcs5$ region around J074749+115352, allowing us to perform the first timing analysis on a timescale of a few hours for an object at the cosmic dawn.

For an accurate timing analysis of J074749+115352, we first apply a barycenter correction to the event, aspect solution (asol1), and exposure statistics (stat1) files, using the Level 1 orbit ephemeris file (eph1) created about one month after the observation (on 2020 February 4; see Table 1 for the observation date). We then extract a 0.5–7 keV light curve of J074749+115352 at a time resolution of 1 ks (Figure 3(a)). The standard deviation of the 0.5–7 keV count rate ($\approx 2.1 \times 10^{-3}$ counts s^{-1}) is $\sim$49% of the mean count rate ($\approx 4.3 \times 10^{-3}$ counts s^{-1}). However, the variance of the light curve shown in Figure 3(a) is even less than the mean square error, resulting in a negative excess variance (Vaughan et al. 2003). This indicates the intrinsic variation is largely embedded in the large statistical noise. More sensitive X-ray observations are needed to confirm whether or not a short timescale variation really exists.

We make some further timing analyses of J074749+115352 to examine the possible time variation of the X-ray spectral properties. Limited by the poor counting statistics, we cannot obtain a high-resolution light curve for a reliable Fourier power

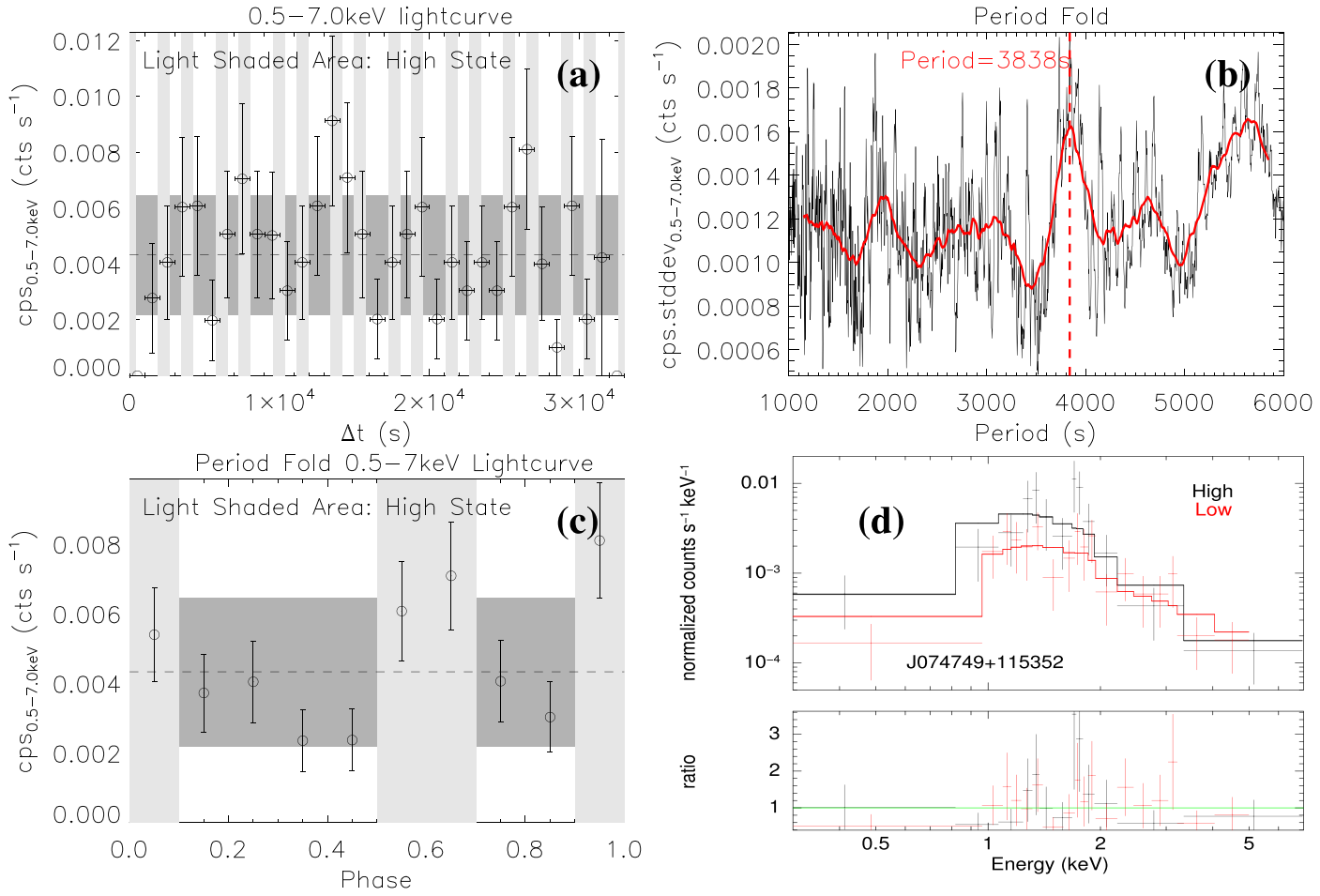

Figure 3. Timing analysis of J074749+115352. All the parameters are measured in the observer's frame. (a) 0.5–7 keV light curve binned to a resolution of 1 ks. The dashed line and the dark shaded area are the mean value and standard deviation of the count rate, respectively. The light shaded area marks the high soft state as analyzed in the other panels. (b) Period folded data to search for the most significant period of the X-ray count rate variations. The *x*-axis is the assumed trial periods, while the *y*-axis is the standard deviation of the 0.5–7 keV count rate of the period folded data. The black curve has been binned to a minimum step of 3 s, while the red curve is a smoothed version of the black curve. The red dashed line is the manually identified peak of the curve at a period of 3838 s. (c) Period folded 0.5–7 keV light curve at an assumed period of 3838 s. The light shaded areas identify the phase of the "high state," with a count rate higher than the mean value (the dashed line and dark shaded area are the same as those in panel (a)). (d) Spectra extracted from the "high" (black) and "low" (red) states identified in (c), respectively. The spectra are analyzed in the same way as those presented in Figure 2.

spectral analysis. In order to test the presence of any possible periodic signal and to search for the most significant variation period, we fold the event file with various trial periods using the CIAO tool *pfold*. At the most significant period, there will be a local peak in the standard deviation of the count rate. We search for such peaks in Figure 3(b), and find the most significant and narrow peak at a period of $P_{\rm obs} \approx 3838$ s in the observer's frame, which corresponds to a period of $P_{\rm rest} \approx 613$ s in the rest frame. We then create a period or phase folded light curve based on this period using the CIAO tool *dmextract* (Figure 3(c)). We identify 0.5 $\leqslant$ phase $<$ 0.7, $\geqslant$0.9, and $<$0.1 as the "High" state typically with a 0.5–7 keV count rate higher than the mean value, while we identify the remaining phases as the "Low" state. The double peak probably indicates there is an unresolved shorter based period of $P_{\rm obs} \sim$ 1900 s, which is, however, much weaker in Figure 3(b). We then create Good Time Intervals (GTIs) for each state with the CIAO tool *dmgti* and align it with *gti_align*. We finally extract the spectra for each phase using *specextract* and analyze them separately in the same way as adopted for the combined spectra above. The best-fit spectra are plotted together in Figure 3(d) and the corresponding X-ray properties of the two phases are summarized in Table 2. We caution that we have adopted the same $L_{2500\,\text{Å}}$ to compute $\alpha_{\rm OX}$ for the "High" and "Low" states of J074749+115352.

3. Discussions

3.1. An Estimate of the Mass of the SMBH in J074749+115352

We first estimate the mass of the SMBH ($M_{\rm SMBH}$) in J074749 +115352 based on the Mg II λ2800 Å emission line. The near-IR spectrum used in the measurement was taken in 2014 March with the TripleSpec spectrograph on the Hale 5 m telescope at the Palomar observatory, with a 1″ slit and a total exposure time of 6000 s (Figure 4). We fit the spectrum with a pseudo-continuum, including a power-law continuum, the Fe II template (Tsuzuki et al. 2006), and the Balmer continuum (De Rosa et al. 2014). The continuum-subtracted spectrum around the Mg II line is fitted with a two-component Gaussian model. The uncertainty is estimated using 50 mock spectra created by randomly adding Gaussian noise at each pixel with its scale equal to the spectral error at that pixel (e.g., Shen et al. 2019; Wang et al. 2020a; Yang et al. 2020). All the 1σ uncertainties are then estimated based on the 16 and 84 percentiles of the distribution. The bolometric luminosity

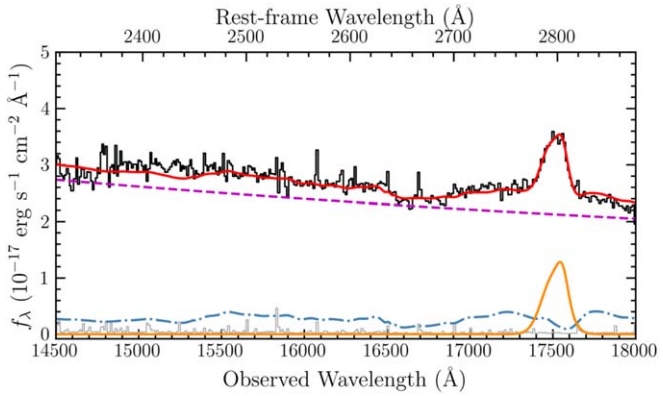

Figure 4. Hale 5 m/TripleSpec H-band spectrum covering the Mg II $\lambda 2800$ Å emission line. The black and gray curves are the observed spectrum and the corresponding uncertainty, respectively. The purple dashed line, blue dashed–dotted curve, and orange solid curve represent the best fits of the power-law continuum, the Fe II template, and the Mg II emission line, respectively. The red solid curve is a sum of the above best-fit model components.

[$L_{\rm bol} = (5.17 \pm 0.21) \times 10^{47}\,{\rm erg\,s^{-1}}$] is estimated from the continuum luminosity at 3000 Å[$L_{3000\,Å} = (3.34 \pm 0.14) \times 10^{43}\,{\rm erg\,s^{-1}\,Å^{-1}}$] with a bolometric correction factor of $\rm BC_{3000} = 5.15$ (Shen et al. 2011). The mass of the SMBH [($M_{\rm SMBH} = (1.82 \pm 0.02) \times 10^9\,M_\odot$)] is then estimated based on $L_{\rm bol}$ and the FWHM of the Mg II line [$(2817 \pm 22)\,{\rm km\,s^{-1}}$] by adopting the local empirical relation from Vestergaard & Osmer (2009). The uncertainty on $M_{\rm SMBH}$ estimated here does not include the systematic uncertainties of the scaling relation, which could be up to ~0.55 dex. We also estimate the corresponding Eddington ratio based on the measured $L_{\rm bol}$ and $M_{\rm SMBH}$, which is $\lambda_{\rm Edd} = 2.25 \pm 0.09$.

3.2. The Possible Short Timescale Variation of J074749+115352

The statistical significance of the X-ray variation of J074749+115352 depends on the time binning of the light curve. A lower time resolution could reduce the statistical uncertainty while it may also reduce the amplitude of the variation, and thus could make the X-ray variation either more or less significant. At some time resolutions such as $\Delta t = 2500$ s, we could get a positive excess variance and a fractional rms variability amplitude of $F_{\rm var} \approx 17\%$ (Vaughan et al. 2003). However, considering the large uncertainties, we conclude that the apparent short timescale variation of J074749+115352 is not statistically significant based on the existing Chandra observations.

After adopting the putative 3838 s period determined in Section 2, distinguishing the X-ray properties of the "High" and "Low" states is quite clear. As shown in Figure 3(d) and listed in Table 2, even if there may be some mixture of photons from different states due to the poorly constrained variation period (also indicated in Figure 3a), the average X-ray flux in the "High" state is still significantly higher than (~2.7 times of) that in the "Low" state ($F_{0.5-2\,\rm keV} = 5.86^{+1.36}_{-1.41} \times 10^{-14}\,{\rm erg\,s^{-1}\,cm^{-2}}$ versus $2.20^{+0.42}_{-0.43}\,{\rm erg\,s^{-1}\,cm^{-2}}$). Furthermore, the X-ray spectrum in the "High" state is also significantly softer ($\Gamma = 2.40^{+0.33}_{-0.32}$ compared to $\Gamma = 1.78^{+0.25}_{-0.24}$ in the low state). Distinguish such "high soft" and "low hard" states is quite common in the X-ray variation of both the SMBHs and stellar mass BHs, which is thought to be mainly caused by the change of the accretion rate (e.g., Nowak 1995; Done & Gierliński 2005). But more data are need to monitor the long-term variation of J074749+115352 in order to better understand the transition of its spectral states.

The short timescale variation detected in J074749+115352 is quite similar to the quasi-periodic oscillation (QPO) observed at low redshifts. Such a short timescale QPO is rarely detected in a quasar hosting such a massive SMBH, which typically shows much longer timescale X-ray variations (e.g., McHardy et al. 2006). Using the scaling relations from González-Martín & Vaughan (2012), the expected variation period of a $\gtrsim 10^9\,M_\odot$ SMBH (Section 3.1) should be about three orders of magnitude of what we have found in J074749+115352 (~70 days adopting its SMBH mass). Therefore, this apparent short timescale variation, if it really exists, cannot be attributed to any ordinary orbital motions of the accretion disk. Gierliński et al. (2008) have discovered an ~1 hour scale QPO in a $z = 0.042$ narrow-line Seyfert 1 galaxy RE J1034+396 (further confirmed by Jin et al. 2020), which hosts an SMBH with a poorly constrained mass of $\sim 10^{5.8-7.6}\,M_\odot$. Jin et al. (2021) further decompose the X-ray emission into four components, including a disk component plus three components (two warm and one hot) from the corona. It is the hotter and less luminous warm corona component producing the QPO. The authors speculate that the QPO is due to the expansion/contraction of the inner disk vertical structure. A more sensitive X-ray telescope, such as the XMM-Newton, is certainly needed for a more reliable spectral-timing analysis to confirm the nature of the X-ray variability of J074749+115352.

3.3. Comparison to Other Quasar Samples

Existing studies have shown a tight correlation between the rest frame UV luminosity of a quasar (typically $L_{2500\,\rm Å}$) and its optical/UV-to-X-ray spectral slope $\alpha_{\rm OX}$ (e.g., Just et al. 2007; Lusso & Risaliti 2016), which traces the relative importance of the emissions from the accretion disk and the corona. We herein compare the three quasars studied in this work to some other surveys of quasars at different redshifts.

There are two major samples plotted in Figure 5 together with the best-fit relation from Just et al. (2007). The Lusso & Risaliti (2016) sample is constructed by cross-matching the SDSS quasar sample with the 3XMM-DR5 catalog of X-ray sources. We only plot their firmly X-ray detected subsample in Figure 5, which consists of 2153 quasars spreading in a broad redshift range of $z < 5$. Lusso & Risaliti's (2016) sample does not include higher-z quasars, which have been increasingly detected in X-ray in recent years (e.g., Nanni et al. 2017; Vito et al. 2018; Salvestrini et al. 2019; Pons et al. 2020; Wang et al. 2020b). We therefore plot another high-z quasar sample from Vito et al. (2019) for comparison, which consists of only $z > 6$ quasars and is certainly biased to the most luminous ones. In addition to these two samples, we also plot two X-ray bright quasars at $z > 6$ recently detected in X-ray, which have relatively flat optical/UV-to-X-ray slope (larger $\alpha_{\rm OX}$), similar as J074749+115352. PSO J030947.49+271757.31 ($z = 6.10$) is the first blazar and also the radio brightest AGN at $z > 6$, with the X-ray emission detected with Swift by Belladitta et al. (2020). CFHQS J142952+544717 is the most distant known radio-loud quasar at $z = 6.18$. Its X-ray emission was detected with eROSITA by Medvedev et al. (2020). It is the X-ray brightest quasar at $z > 5$ with an X-ray flux about twice that of J074749+115352.

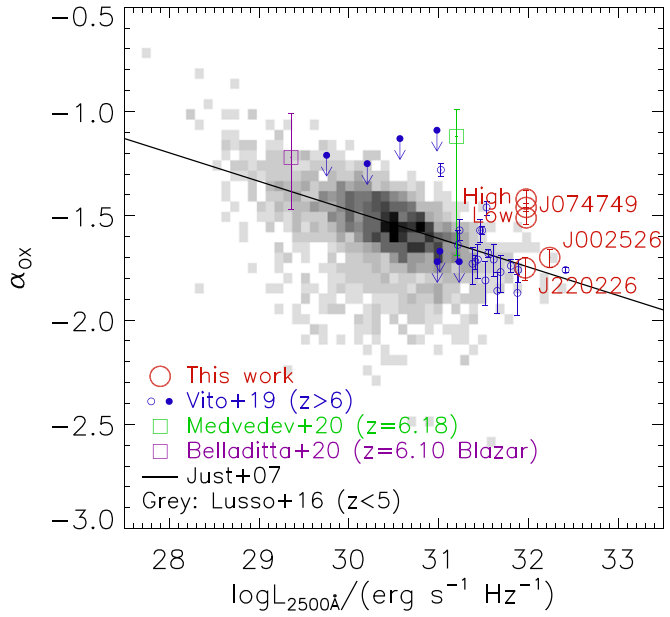

Figure 5. Comparison of our $z \gtrsim 5$ quasars with other quasar samples on the well defined $L_{2500\,Å} - \alpha_{OX}$ relation. The three quasars studied in this work, as well as the "High" and "Low" states of J074749-115352 are plotted with large red open circles. The error bars are smaller than the size of the symbols. Blue dots are the $z > 6$ quasars from Vito et al. (2019). The open ones denote firm X-ray detections, while solid ones denote upper limits on X-ray detections. The purple and green boxes are the recent discovery of two X-ray bright quasars at $z > 6$ from Belladitta et al. (2020) and Medvedev et al. (2020), respectively. The quasar from Medvedev et al. (2020) is the X-ray brightest one known at $z > 5$, while J074749+115352 from this work is the second X-ray brightest. Gray shaded pixels are a large sample of 2153 firmly X-ray detected quasars at $z < 5$ from Lusso & Risaliti (2016). The darkness of the pixel is proportional to the number of quasars in the corresponding $L_{2500\,Å}$ and α_{OX} bins. We discarded their upper limits on X-ray nondetected sources to avoid confusion. The solid line is the best-fit relation from Just et al. (2007; see Figure 7 in their paper).

As shown in Figure 5, two of the three quasars studied in this work, J002526-014532 and J220226+150952, are consistent with the $L_{2500\,Å} - \alpha_{OX}$ relation defined with low-z quasars and most of the $z > 6$ quasars (many of Vito et al.'s 2019 quasars with large α_{OX} are upper limits). Their relatively high X-ray luminosity is only a result of their high UV luminosity. However, J074749+115352 appears to be extraordinarily X-ray bright at its UV luminosity, as indicated by the significantly larger α_{OX} than the best-fit relation. Adopting a bolometric luminosity of $L_{bol} \sim 5 \times 10^{47}$ erg s^{-1} roughly estimated from the M_{1450}, J074749+115352 is ~4 times as bright as expected from the $L_{bol} - L_X$ scaling relation (Wang et al. 2020b; similar to that predicted from a $L_{UV} - L_X$ relationship, e.g., Salvestrini et al. 2019).

X-ray observations from AGNs are expected to be suppressed compared to the UV luminosity when the Eddington ratio is high (e.g., Jiang et al. 2019). Observations indicate an increasing bolometric correction factor in the X-ray band (i.e., a higher bolometric to X-ray luminosity ratio) with the increasing Eddington ratio or bolometric luminosity (e.g., Lusso et al. 2012; Duras et al. 2020). We do not have a measurement of the SMBH mass and Eddington ratio for J002526-014532 and J220226+150952. Adopting the average rest frame 2–10 keV luminosity of $L_{2-10\,keV} = (1.22 \pm 0.16) \times 10^{46}$erg s^{-1} (Table 2) and the bolometric luminosity of $L_{bol} = (5.17 \pm 0.21) \times 10^{47}$erg s^{-1} $= (1.35 \pm 0.05) \times 10^{14} L_\odot$ for J074749+115352 (Section 3.1), we obtain a 2–10 keV bolometric correction factor of $L_{bol}/L_{2-10\,keV} = 42.4 \pm 5.8$. At the Eddington ratio of $\lambda_{Edd} \sim 2$ or the bolometric luminosity of $L_{bol} \sim 10^{14} L_\odot$ for J074749+115352, the expected X-ray bolometric correction factor is typically $L_{bol}/L_{2-10\,keV} > 60$ based on the $L_{bol}/L_{2-10\,keV} - \lambda_{Edd}$ relationship from Lusso et al. (2012), or $L_{bol}/L_{2-10\,keV} > 100$ based on the $L_{bol}/L_{2-10\,keV} - L_\odot$ relationship from Duras et al. (2020). J074749+115352 is radio-quiet so the strong X-ray emission is unlikely to be produced by the jet (Yang et al. 2016). We therefore conclude that this quasar is extraordinarily X-ray bright compared to most of the AGNs.

As an important probe of the accretion physics, there are a few studies of the redshift evolution of the X-ray spectral slope of high-z quasars (e.g., Vito et al. 2019; Wang et al. 2020b). Although there are still very few measurement of Γ for high-z quasars ($\lesssim$20 for $z > 5$ quasars), we notice that a constant X-ray spectral slope of $\Gamma \approx 1.9$ at $z < 6$ has been claimed, with a steeper average X-ray spectral slope (larger Γ) at $z \gtrsim 6$. The increase of Γ at $z \gtrsim 6$, however, is probably caused by the higher λ_{Edd} of the $z \gtrsim 6$ quasar samples (Wang et al. 2020b). We add reliable X-ray measurements of Γ of three quasars into the sample of $z \sim 5$ quasars. The X-ray spectral slope of our quasars (the best-fit Γ is in the range of 1.6–2.1) is consistent with the average Γ of $z = 4$–6 quasars, considering the error of the measurement and the dependence on the unknown λ_{Edd} (currently only J074749+115352 has an estimate of λ_{Edd}). We therefore do not find a significant redshift evolution of Γ based on the existing X-ray data.

4. Summary

In this paper, we report new Chandra observations of three $z \sim 5$ quasars, which are the UV brightest radio-quiet ones at the corresponding redshift. Significant X-ray emissions have been clearly detected and a high-quality X-ray spectrum can be extracted to measure the basic X-ray properties of each quasar. All three quasars have a rest frame 2–10 keV luminosity $L_{2-10\,keV} > 10^{45}$ erg s^{-1} and the X-ray power-law photon index is well constrained (Γ in the range of 1.6-2.1). In particular, we confirm that J074749+115352 is the X-ray brightest radio-quiet quasar at $z > 5$ with an average observed X-ray flux $F_{0.5-2\,keV} = 3.49^{+0.44}_{-0.45} \times 10^{-14}$ erg s^{-1} cm^{-2} (or a mean Chandra/ACIS-S count rate $cps_{0.5-7\,keV} \approx 4.3 \times 10^{-3}$ counts s^{-1}).

The high X-ray flux of J074749+115352 makes it unique for timing analysis on a timescale of a few hours at such high redshift. We find that J074749+115352 may have some short timescale variations, although such variations may be embedded in the large statistical noise. The best-fit period in the observer's frame is $P_{obs} \approx 3838$ s with a corresponding rest frame period of $P_{rest} \approx 613$ s. We extract a period folded light curve and phase folded spectra, and find that there are two clearly distinguishable states in the X-ray variation: a "high soft" state with an average X-ray flux ~2.7 times of the "low hard" state, and the X-ray spectral slope is also significantly steeper ($\Gamma = 2.40^{+0.33}_{-0.32}$ versus $1.78^{+0.25}_{-0.24}$). We also estimate the mass of the SMBH in J074749+115352 based on a near-IR spectrum covering the Mg II λ2800 Å emission line, which is $M_{SMBH} = (1.82 \pm 0.02) \times 10^9 M_\odot$. This is the first detection of a possible X-ray variation on a timescale of a few kiloseconds around such a massive SMBH at such a high redshift; though, more sensitive X-ray observations are needed to examine this short timescale X-ray variation.

We also compare the three quasars detected in this paper to other quasar samples. We find that J074749+115352 is extraordinarily X-ray bright, with an average $\alpha_{\rm OX} = -1.46 \pm 0.02$ and 2–10 keV bolometric correction factor $L_{\rm bol}/L_{\rm 2-10\ keV} = 42.4 \pm 5.8$, both significantly departing from some well defined scaling relations. This quasar also has a high Eddington ratio of $\lambda_{\rm Edd} = 2.25 \pm 0.09$. More X-ray and IR observations are needed to confirm the nature and to better understand the properties of this unique quasar at the end of the cosmic dawn. This work has added reliable X-ray measurements of Γ for three quasars at $z \sim 5$, but we do not find a significant redshift evolution of Γ based on the existing limited sample of high-z quasars with high-quality X-ray data.

The authors would like to acknowledge the anonymous referee for helpful comments and suggestions. We acknowledge Dr. Abderahmen Zoghbi at the University of Michigan for helpful discussions on the timing analysis of J074749+115352. The authors also acknowledge the use of data obtained at the Palomar 5.1 m telescope. J.T.L. acknowledge the financial support of this project from NASA and the Smithsonian Institution through grant GO0-21097X, as well as general financial support from NASA through grant 80NSSC19K0579 and from the Smithsonian Institution through grants GO9-20074X and AR9-20006X. F.W. is thankful for the support provided by NASA through the NASA Hubble Fellowship grant #HST-HF2-51448.001-A awarded by the Space Telescope Science Institute, which is operated by the Association of Universities for Research in Astronomy, Incorporated, under NASA contract NAS5-26555.

ORCID iDs

Jiang-Tao Li https://orcid.org/0000-0001-6239-3821
Feige Wang https://orcid.org/0000-0002-7633-431X
Jinyi Yang https://orcid.org/0000-0001-5287-4242
Yuming Fu https://orcid.org/0000-0002-0759-0504
Fuyan Bian https://orcid.org/0000-0002-1620-0897
Joel N. Bregman https://orcid.org/0000-0001-6276-9526
Xiaohui Fan https://orcid.org/0000-0003-3310-0131
Qiong Li https://orcid.org/0000-0002-3119-9003
Xue-Bing Wu https://orcid.org/0000-0002-7350-6913

References

An, H., & Romani, R. W. 2020, ApJ, 904, 27
Bañados, E., Venemans, B. P., Mazzucchelli, C., et al. 2018, Natur, 553, 473
Belladitta, S., Moretti, A., Caccianiga, A., et al. 2020, A&A, 635L, 7
De Rosa, G., Venemans, B. P., Decarli, R., et al. 2014, ApJ, 790, 145
Done, C., & Gierliński, M. 2005, MNRAS, 364, 208
Duras, F., Bongiorno, A., Ricci, F., et al. 2020, A&A, 636, 73
Gierliński, M., Middleton, M., Ward, M., & Done, C. 2008, Natur, 455, 369
González-Martín, O., & Vaughan, S. 2012, A&A, 544, 80
HI4PI Collaboration, Ben Bekhti, N., Flöer, L., et al. 2016, A&A, 594, 116
Jiang, Y.-F., Stone, J. M., & Davis, S. W. 2019, ApJ, 880, 67
Jin, C., Done, C., & Ward, M. 2020, MNRAS, 495, 3538
Jin, C., Done, C., & Ward, M. 2021, MNRAS, 500, 2475
Just, D. W., Brandt, W. N., Shemmer, O., et al. 2007, ApJ, 665, 1004
Lusso, E., Comastri, A., Simmons, B. D., et al. 2012, MNRAS, 425, 623
Lusso, E., & Risaliti, G. 2016, ApJ, 819, 154
McConnell, N. J., Ma, C.-P., Gebhardt, K., et al. 2011, Natur, 480, 215
McHardy, I. M., Koerding, E., Knigge, C., Uttley, P., & Fender, R. P. 2006, Natur, 444, 730
Medvedev, P., Sazonov, S., Gilfanov, M., et al. 2020, MNRAS, 497, 1842
Nanni, R., Vignali, C., Gilli, R., Moretti, A., & Brandt, W. N. 2017, A&A, 603, 128
Nowak, M. A. 1995, PASP, 107, 1207
Pons, E., McMahon, R. G., Banerji, M., & Reed, S. L. 2020, MNRAS, 491, 3884
Romani, R. W. 2006, AJ, 132, 1959
Salvestrini, F., Risaliti, G., Bisogni, S., Lusso, E., & Vignali, C. 2019, A&A, 631, 120
Shen, Y., Richards, G. T., Strauss, M. A., et al. 2011, ApJS, 194, 45
Shen, Y., Wu, J., Jiang, L., et al. 2019, ApJ, 873, 35
Smidt, J., Whalen, D. J., Johnson, J. L., Surace, M., & Li, H. 2018, ApJ, 865, 126
Timlin, J. D., III, Brandt, W. N., Zhu, S., et al. 2020, MNRAS, 498, 4033
Trakhtenbrot, B., Netzer, H., Lira, P., & Shemmer, O. 2011, ApJ, 730, 7
Tsuzuki, Y., Kawara, K., Yoshii, Y., et al. 2006, ApJ, 650, 57
van den Bosch, R. C. E., Gebhardt, K., Gültekin, K., et al. 2012, Natur, 491, 729
Vaughan, S., Edelson, R., Warwick, R. S., & Uttley, P. 2003, MNRAS, 345, 1271
Vestergaard, M., & Osmer, P. 2009, ApJ, 699, 800
Vito, F., Brandt, W. N., Bauer, F. E., et al. 2019, A&A, 630, 118
Vito, F., Brandt, W. N., Yang, G., et al. 2018, MNRAS, 473, 2378
Wang, F., Davies, F. B., Yang, J., et al. 2020a, ApJ, 896, 23
Wang, F., Fan, X., Yang, J., et al. 2020b, ApJ, submitted (arXiv:2011.12458)
Wang, F., Wu, X.-B., Fan, X., et al. 2016, ApJ, 819, 24
Willott, C. J., Albert, L., Arzoumanian, D., et al. 2010, AJ, 140, 546
Wu, X.-B., Wang, F., Fan, X., et al. 2015, Natur, 518, 512
Yang, J., Fan, X., Wu, X.-B., et al. 2017, AJ, 153, 184
Yang, J., Wang, F., Fan, X., et al. 2020, ApJL, 897, 14
Yang, J., Wang, F., Wu, X.-B., et al. 2016, ApJ, 829, 33